ELSEVIER

Thermochimica Acta 314 (1998) 255–263

thermochimica acta

Thermodynamics of liquid Al–Ni alloys

K.V. Grigorovitch[a,*], A.S. Krylov[b]

[a] *Baikov Metallurgy Institute, RAS, Leninsky pr. 49, 117911 Moscow, Russian Federation*
[b] *Faculty of Computational Mathematics and Cybernetics, Moscow State University, Leninskie Gory, 119899 Moscow, Russian Federation*

Received 10 October 1997; accepted 6 January 1998

Abstract

A new high-temperature calorimeter was used to study the enthalpies of mixing of nickel-rich Al–Ni melts (mole fraction of Al<0.22) at 1823 K. Concentration dependencies of the partial and integral enthalpies of dissolution of aluminium were obtained experimentally. The model of quasi-ideal associated solutions and ASSOL-2 original software were used to treat and evaluate all available thermodynamic data for liquid Al–Ni system. The description of thermodynamic properties of liquid Al–Ni alloys in a wide concentration and temperature intervals was obtained. © 1998 Published by Elsevier Science B.V.

Keywords: Al–Ni melt; Enthalpy of mixing; Calorimetry; Thermodynamics; Associated solution

1. Introduction

The binary Al–Ni system is very important in connection with a wide application of nickel-base superalloys containing a substantial percentage of aluminium. Characteristic of the binary Al–Ni system phase diagram [1,2] is the formation of an ordered BCC β' AlNi phase isotypic with CsCl, from typically FCC metals. The melting temperature of β'-AlNi is higher than the melting temperatures of the constituent metals. The Al–Ni phase diagram has five intermediate compounds: ε-Al_3Ni (orthorhombic), δ-Al_3Ni_2 (trigonal), β' AlNi (BCC), α'-Al_3Ni_5 (orthorhombic) and α''-$AlNi_3$ (FCC ordered phase). The solid solubility of nickel in aluminium is very small and increases with temperature from 0.01 at.% (773 K) to 0.11 at.% at the eutectic temperature (913 K). Ni has a wide γ solid solution range with significant solubility of aluminium up to 21.1 at.% at the eutectic temperature (1658 K). The decrease of the terminal solubility of aluminium in the γ-solid solution with decrease of the temperature results in precipitation of the intermetallic $AlNi_3$ phase and strengthening of these alloys. The presence of a congruently melting compound, AlNi, suggests a strong interaction in liquid Al–Ni system and hence high absolute values of enthalpies of mixing.

The Al–Ni phase diagram is of fundamental interest for alloys, containing the $AlNi_3$ phase in the α-matrix, the α/α' two-phase field (Ni-rich part), and for glass forming alloys (Al-rich part).

The thermodynamics of the Al–Ni liquid alloys were thoroughly investigated in wide concentration and temperature intervals [3–13]. Different experimental techniques were used – the partition of aluminium between Ag and Al–Ni alloys [3], EMF concentration cell methods [6,11], high temperature

*Corresponding author.

PII S0040-6031(98)00262-7

Table 1
Review of thermodynamic determination of chemical activities and activity coefficients (a_{Ni}, a_{Al}, γ_{Al}), partial enthalpies ($\Delta\bar{H}_{Ni}, \Delta\bar{H}_{Al}$) of nickel and aluminium, integral mixing enthalpies (ΔH), concentration and temperature range of the investigations, the method employed (Partition of Al between Ag and Al–Ni alloys, EMF – electromotive force, high temperature calorimetry, Knudsen effusion mass spectrometry), years and references

Measured values	Temperature range (K)	Concentration range (N_{Al})	Method employed	Reference, Year
a_{Al}	1873	0.05–0.4	Partition of Al	[3], 1965
$\Delta\bar{H}_{Ni}, \Delta\bar{H}_{Al}$	1923	0–1.0	Calorimetric	[4], 1971
$\Delta\bar{H}_{Al}$	1873	0, 0.25, 0.75	Calorimetric	[5], 1976
a_{Al}, γ_{Al}	1100	0.847–0.995	EMF	[6], 1979
$\Delta\bar{H}_{Ni}, \Delta\bar{H}_{Al}$	1773	0.05–0.5	Calorimetric	[7], 1983
$\Delta\bar{H}_{Ni}$	1158	0.989–0.998	Calorimetric	[8], 1985
a_{Ni}	1750–2100	0.11–0.46	Knudsen EMS	[9], 1980
$\Delta\bar{H}_{Al}, \Delta H$	1800	0.5–1.0	Calorimetric	[10], 1990
a_{Al}	1173	0.849–0.952	EMF	[11], 1989
a_{Al}, a_{Ni}	1728	0.06–0.27	Knudsen EMS	[12], 1990
ΔH	1700	0.22, 0.27, 0.7–0.88	Calorimetric	[13], 1993

mixing calorimetry [4,5,7,8,10,13] and Knudsen effusion mass spectrometry (EMS) [9,12].

Table 1 gives a review of thermodynamic studies for the determination of chemical activities and activity coefficients (a_{Ni}, a_{Al}, γ_{Al}), partial enthalpies ($\Delta\bar{H}_{Ni}$, $\Delta\bar{H}_{Al}$) of nickel and aluminium, integral enthalpies of mixing, concentration and temperature range of the investigations, the method employed, years and references.

The comparison and estimation of the reliability of different experimental data sets of partial and integral enthalpies and activities of the components is impossible without additional computational analysis. The analysis of the experimental data given in [14] was an empiric one.

The available data on the enthalpy of mixing of Al–Ni melts are far from being complete. In this connection, further investigation of metallic solutions using new calorimetric equipment and software is an actual problem.

Therefore the purposes of this investigation were:

- to measure the partial and integral enthalpy of mixing of the Al–Ni system using a high temperature calorimeter,
- to obtain a reliable thermodynamic description of the binary system in liquid phase by a model approach using the original model of quasi-ideal associated solutions (QIAS) and ASSOL-2 software, based on existing experimental data sets.

2. Experimental

High-temperature calorimetry is one the most important methods of thermodynamic investigation of liquid alloys. It provides a direct determination of the enthalpy of mixing of melts.

The high temperature isoperibolic mixing calorimeter [15] was used for the experiments. The apparatus consists of the vacuum resistance furnace, vacuum system, inert gas purification and bleeding-in system, temperature measuring and control system. The calorimeter consists of a molybdenum sheet heater located inside a water-cooled shell and a reflecting screens system. A tungsten–rhenium thermocouple was used for monitoring the heater temperature. The calorimeter shell temperature was maintained constant, the temperature of the calorimetric body (alumina crucible with melt) was a function of the thermal effect of the mixing reaction. The enthalpies were calculated from the difference of the calorimetric body and shell temperatures as a function of time.

As shown in Fig. 1 the calorimetric cell consists of a massive molybdenum block (1) and a measuring cell located in the isothermal zone of the heater. The massive molybdenum block consists of the lower part and cover (2). Specimens of alloys were dropped into the crucible out of a feeder along a system of guide tubes (3). The temperature of the block was measured with a tungsten–rhenium thermocouple (7).

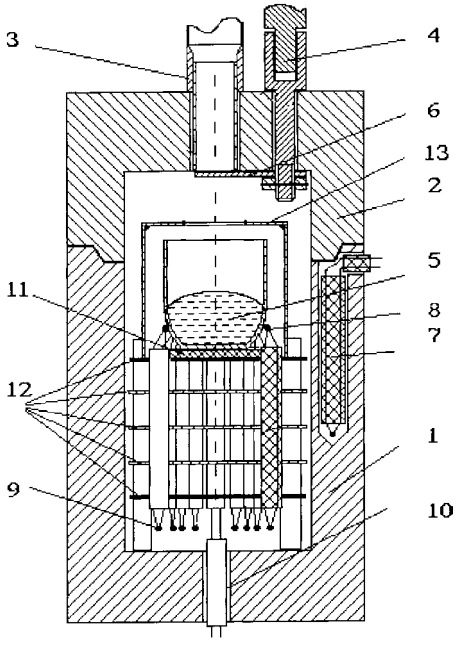

Fig. 1. The calorimetric cell: 1,2-lower part and cover of the molybdenum block, respectively; 3-guide tubes system; 4-tungsten gate drive; 5-alumina crucible with melt; 6-tungsten gate; 7-tungsten–rhenium thermocouple; 8,9-measuring and reference junctions of the tungsten–rhenium thermocouples battery, respectively; 10-output of the thermocouples battery; 11-refractory reflecting screen; 12 and 13-molybdenum reflecting screens.

Twelve tungsten–rhenium thermocouples in series measured the heat effect of dissolution. The measuring junctions (8) surround the crucible with the melt (5). The reference junctions (9) are positioned close to the bottom of the massive block. The refractory (11) and molybdenum reflecting screens (12) provide the heat-transfer resistance between the measuring and reference junctions.

The weight of the melt and the specimen dropped were 5–30 and 0.03–0.20 g, respectively. The sensitivity of the calorimeter at 1823 K was of the order of 0.1 mV/W.

The calorimeter was evacuated before the experiments to a pressure of approximately 10^{-2} Pa. The furnace was heated up to 1173–1273 K for degassing, then high-purity argon was bled-in to build up an excess pressure of about 104 Pa to prevent seeking-in of oxygen. Titanium getters were used in the hot zone for additional removal of oxygen. The temperature of the heater was stabilised automatically accurate to ±0.1 K using a precision temperature regulator.

The experiment involved firstly dropping of the solvent specimens, then the specimens of the component to be dissolved. The specimens were preliminary weighed accurate to 0.1 mg using a precise balance. The thermobattery signal generated by the heat effect of the dissolution process was registered with a recorder and integrated in a precision digital integrator.

The results of experiments were processed with the heat balance equation of an isoperibolic calorimeter [15]:

$$C\frac{\mathrm{d}\Delta T}{\mathrm{d}\tau} = \frac{\mathrm{d}Q_1}{\mathrm{d}\tau} + \frac{\mathrm{d}Q_2}{\mathrm{d}\tau} \tag{1}$$

where τ is the time, in s, ΔT in K is the difference of calorimetric cell and the shell temperatures, C in kJ/K is the effective heat capacity of the calorimeter, $\frac{\mathrm{d}Q_1}{\mathrm{d}\tau}$ in W is the power of the dissolution thermal effect, $\frac{\mathrm{d}Q_2}{\mathrm{d}\tau}$ in W is the power of the heat exchange between the calorimetric cell and shell.

The heat exchange was described by Newton's linear relationship, because of the small difference between the calorimeter and shell temperatures (ΔT):

$$\frac{\mathrm{d}Q_2}{\mathrm{d}\tau} = K\Delta T \tag{2}$$

where K in W/K is the heat exchange constant. It was experimentally shown, that Eq. (2) could be applied if the temperature difference ΔT does not exceed 4–5 K. The weight of specimens was preliminary adjusted so that the temperature drop was within 3–5 K.

The heat of dissolution was obtained by substituting (2) in the heat balance Eq. (1) and by integrating with respect to time:

$$Q_1 = K\int_0^\infty \Delta T(\tau)\mathrm{d}\tau = WF, \tag{3}$$

where F is the area bounded by the time–temperature curve $\Delta T(\tau)$ in area units and K is the heat exchange coefficient in kJ/(area unit). The weight and volume of the melt increase during the experiment, therefore the heat exchange coefficient is not constant. Its initial value was found by dropping cold specimens of the solvent into the calorimeter.

Based on Eq. (3) the system of equations for calculating the enthalpies of formation in the Al–Ni binary was:

$$\Delta\bar{H}_1(N_1) = -\Delta H^T_{1,T_0} + K(N_1)F_1(N_1) \quad (4)$$

$$\Delta\bar{H}_2(N_1) = -\Delta H^T_{2,T_0} + K(N_1)F_2(N_1), \quad (5)$$

$$\Delta H(N_1) = (1-N_1)\Delta\bar{H}_1(N_1) + N_1\Delta\bar{H}_2(N_1), \quad (6)$$

where N_1 is the atomic fraction of aluminium, $\Delta\bar{H}_1(N_1)$, $\Delta\bar{H}_2(N_1)$ and $\Delta H(N_1)$ are the partial and integral enthalpies of dissolution in kJ/g-atom, $\Delta H^T_{1,T_0}$ and $\Delta H^T_{2,T_0}$ are the enthalpies of the components between the initial temperature T_0 and the considered temperature T in kJ/g-atom, $F_1(N_1)$ and $F_2(N_1)$ are the concentration dependencies of the specific (i.e., referred to one mole) areas bounded by the measured signal curves in (area unit)/g-atom and $K(N_1)$ is the concentration dependence of the calorimeter thermal constant. The product $K(N_1)F_1(N_1)$ is the measured heat change after dropping the specimen. The system of equations refers to one mole of the solution.

Based on the Gibbs-Duhem equation the coefficient K was determined [15]:

$$K(N_1) = \frac{\Delta H^T_{1,T_0}}{F_1(N_1)(1-N_1) + N_1F_2(N_1)} \exp\left(-\int_0^{N_1} \frac{(F_1(y) - F_2(y))\mathrm{d}y}{F_1(y)(1-y) + yF_2(y)}\right) \quad (7)$$

Pure (99.99%) nickel and aluminium were used for experiments. Pure liquid aluminium was taken as standard state and the enthalpy of melting of aluminium (10.2 kJ/mol) was used. The initial partial enthalpy of dissolution of aluminium in nickel was found to be −158.1 kJ/g-atom. The integral enthalpies of mixing at 1873 K are given in Table 2.

Table 2
Experimental values of integral mixing enthalpy of Al–Ni at 1823 K

N_{Al}	ΔH (kJ·mol^{-1})
0.02	−3.09
0.04	−6.19
0.06	−9.29
0.08	−12.39
0.10	−15.47
0.12	−18.53
0.14	−21.56
0.16	−24.56
0.18	−27.49
0.20	−30.37
0.22	−33.19

3. Thermodynamic model and results of calculation

The model of quasi-ideal associated solutions (QIAS) ([16], [17]) was used to treat the available thermodynamic data for liquid Al–Ni. The melt is assumed to contain 'associate' A_mB_k and nonassociated particles A and B in dynamic equilibrium:

$$A_mB_k \leftrightarrow mA + kB \quad (8)$$

The associate dissociation constant by the model is

$$K = \frac{(X_A)^m(X_B)^k}{X_{A_mB_k}}, \ \ln K = C_1/T + C_2 \quad (9)$$

and

$$\frac{(\psi_A)^m(\psi_B)^k}{\psi_{A_mB_k}} = 1 \quad (10)$$

where, X_A, X_B and $X_{A_mB_k}$ and, ψ_A, ψ_B and $\psi_{A_mB_k}$ are the mole fractions and activity coefficients of the association solution components, respectively.

The existence of AlNi associates (m=k=1, A≡Al, B≡Ni, AB≡AlNi) was assumed, because of the strong negative enthalpy of mixing with the triangular shape of the curve and a minimum at the equiatomic composition, and the existence of the high melting intermetallic phase AlNi. This type of the associate was also assumed in [13].

For this case, the equations of the QIAS model are:

$$X_{AlNi} = \frac{(K + N_1^2 + N_2^2 - \sqrt{(K+N_1^2+N_2^2)^2 - 4N_1^2N_2^2})}{2N_1N_2} \quad (11)$$

$$RT\ln\psi_{Al} = N_2^2(\Phi_{12}(1-2N_1) + 2\Phi_{21}N_1), \quad (12)$$

$$RT\ln\psi_{Ni} = N_1^2(\Phi_{21}(1-2N_2) + 2\Phi_{12}N_2) \quad (13)$$

and

$$a_1 = \gamma_1 N_1 = \psi_{\mathrm{Al}} X_{\mathrm{Al}} \quad (14)$$

$$a_2 = \gamma_2 N_2 = \psi_{\mathrm{Ni}} X_{\mathrm{Ni}} \quad (15)$$

$$X_{\mathrm{Al}} = N_1 - N_2 X_{\mathrm{AlNi}} \quad (16)$$

$$X_{\mathrm{Ni}} = N_2 - N_1 X_{\mathrm{AlNi}} \quad (17)$$

where $N_1 \neq 0$ and $N_2 \neq 0$ are the mole fractions, a_1 and a_2 are the activities, and γ_1 and γ_2, the activity coefficients of components 1 (Al) and 2 (Ni), respectively. The corresponding parametrization of excess molar energy, integral and partial excess thermodynamic functions in the general case are presented in [17]. Here we used the following formulae for the integral enthalpy of mixing:

$$\Delta H = N_1 N_2 (\Phi_{12} N_2 + \Phi_{21} N_1) + RC_1 X_{\mathrm{AlNi}} / (1 + X_{\mathrm{AlNi}}) \quad (18)$$

the partial enthalpies of mixing:

$$\Delta \bar{H}_i = \Phi_{ij} N_j^2 (N_j - N_i) + 2\Phi_{ji} N_i N_j^2 + \frac{C_1 R X_{\mathrm{AlNi}}}{1 + X_{\mathrm{AlNi}}} \left[1 + (-1)^i N_j \frac{X_{\mathrm{Al}} - X_{\mathrm{Ni}}}{X_{\mathrm{Al}} X_{\mathrm{Ni}} + X_{\mathrm{AlNi}} (X_{\mathrm{Ni}} - (X_{\mathrm{Ni}} - X_{\mathrm{Al}}) N_1)} \right] \quad (19)$$

where $j=2$ for $i=1$, and $j=1$ for $i=2$;

excessive heat capacity:

$$\Delta C_{\mathrm{p}} = -(C_1/T)^2 R X_{\mathrm{Al}} X_{\mathrm{Ni}} X_{\mathrm{AlNi}} / [(1 + X_{\mathrm{AlNi}})^2 \times (X_{\mathrm{Al}} X_{\mathrm{Ni}} - N_1 X_{\mathrm{Ni}} - N_2 X_{\mathrm{Al}})] \quad (20)$$

Darken's [18] stability function:

$$\mathrm{St} = \frac{\mathrm{d}^2 \Delta G^{\mathrm{ex}}}{\mathrm{d}N_2^2} = \frac{RT}{N_1 X_{\mathrm{Ni}}} \left(1 + X_{\mathrm{AlNi}} - N_1 \frac{\mathrm{d}X_{\mathrm{AlNi}}}{\mathrm{d}N_2} \right) + 6N_2 (\Phi_{21} - \Phi_{12}) + 2(\Phi_{12} - 2\Phi_{21})$$

$$\frac{\mathrm{d}X_{\mathrm{AlNi}}}{\mathrm{d}N_2} = \frac{X_{\mathrm{AlNi}} (1 + X_{\mathrm{AlNi}}) \left(\frac{1}{X_{\mathrm{Ni}}} - \frac{1}{X_{\mathrm{Al}}} \right)}{\left[1 + X_{\mathrm{AlNi}} \left(\frac{1}{X_{\mathrm{Al}}} + \left(\frac{1}{X_{\mathrm{Ni}}} - \frac{1}{X_{\mathrm{Al}}} \right) N_1 \right) \right]} \quad (22)$$

and the Bhatia–Thornton [19] partial concentration structure factor in the long wavelength limit:

$$S_{\mathrm{cc}}(0) = RT/\mathrm{St} \quad (23)$$

The use of this model for the case of ternary melts was described in [20].

To determine the parameters Φ_{12}, Φ_{21}, C_1 and C_2, based on a set of experimental data, a minimization of the function was carried out

$$F^2 = \frac{1}{n_{\mathrm{p}}} \sum_{i=1}^{n_{\mathrm{p}}} \left[\frac{(y_i^{\mathrm{c}} - y_i^{\mathrm{e}})^2}{(y_i^{\mathrm{e}})^2} \right] \quad (24)$$

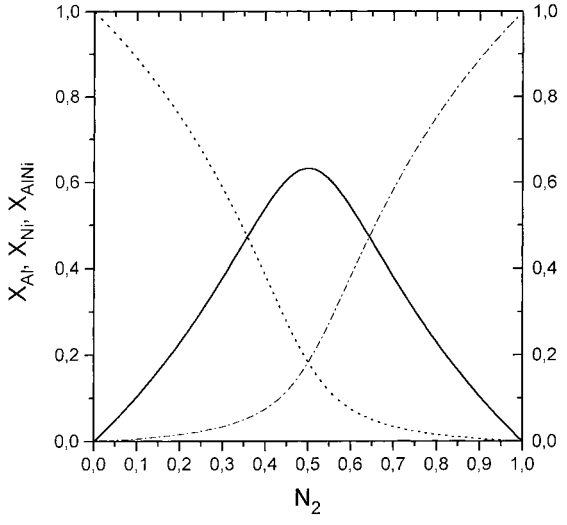

Fig. 2. Mole fractions of Al (• • •), Ni (– • –) and AlNi (———) associate as calculated by the QIAS model at 1800 K.

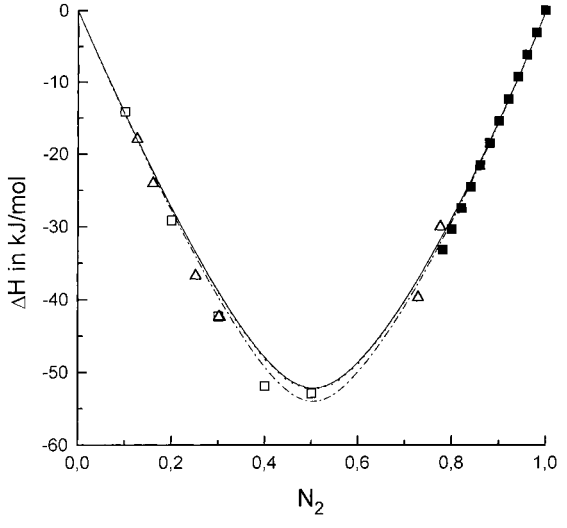

Fig. 3. Integral enthalpy of mixing ΔH calculated by QIAS model (———: T=1823 K, • • •: T=1800 K, – • –: T=1700 K) and experimental data (■: data of this work at 1823 K, □: [10] at 1800 K, and Δ: [13] at 1700 K).

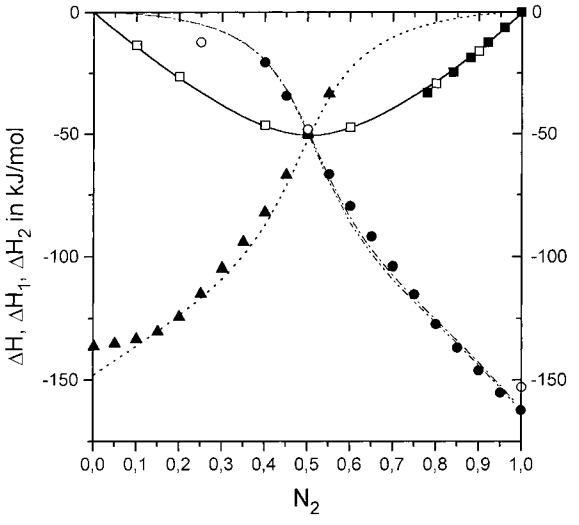

Fig. 4. Integral enthalpy of mixing ΔH at 1923 K (———: calculated by QIAS model, □: [4]) and at 1823 K ■: data of this work), partial enthalpy of Ni $\Delta\bar{H}_2$ at 1923 K (• • •: by QIAS model, ▲: [4]), and partial enthalpy of Al $\Delta\bar{H}_1$ at 1923 K(–• –: by QIAS model, ●: [4]) and at 1873 K (–●●–: by QIAS model, ○: [5]).

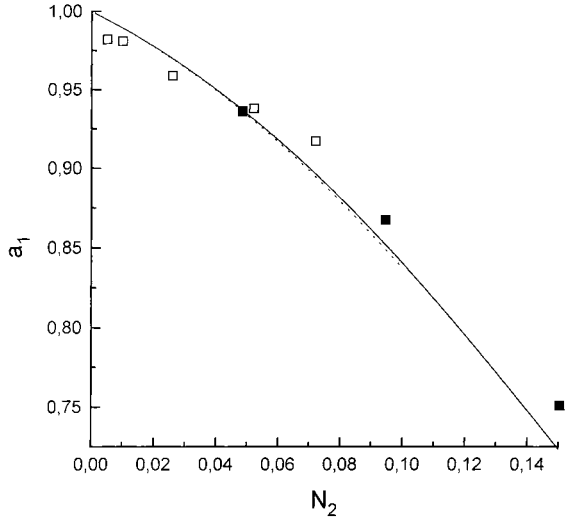

Fig. 5. Activity of Al calculated by QIAS model (———: T=1173 K, • • •: T=1100 K) and experimental data (■: [11] at T=1173 K and □: [6] at 1100 K).

where y_i^e were the experimental enthalpies of mixing or component activities, y_i^c are the quantities calculated by QIAS model, and n_p is the number of experimental points. The minimization was performed

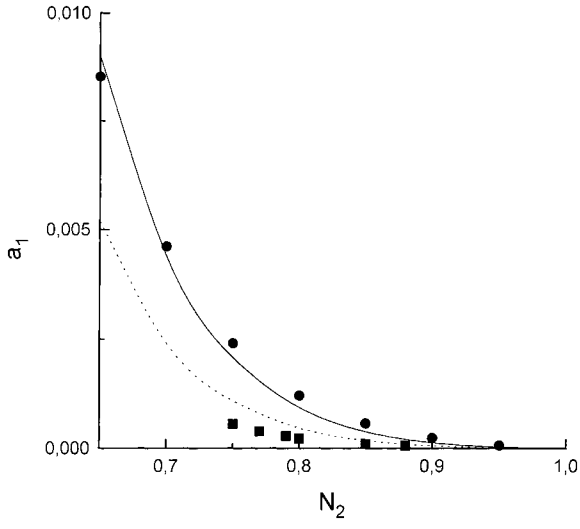

Fig. 6. Activity of Al calculated by QIAS model (———: T=1873 K, • • •: T=1728 K) and experimental data (●: [3] at T=1873 K and ■: [12] at 1728 K).

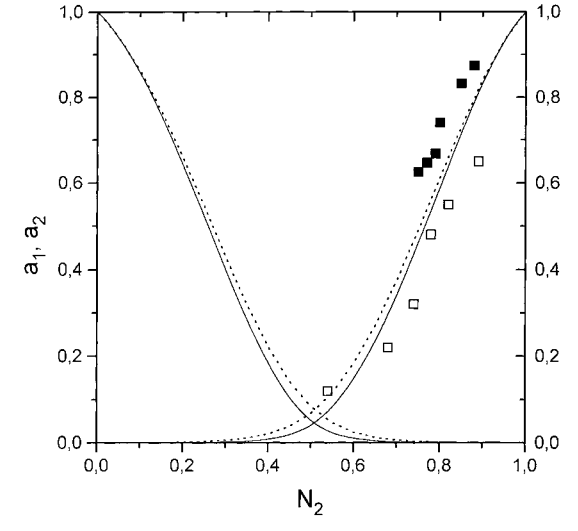

Fig. 7. Activities of Al and Ni calculated by QIAS model (———: T=1728 K, • • •: T=2000 K) and experimental activity of Ni (■: [12] at T=1728 K and □: [9] at 2000 K).

using a variant of Newton–Gauss method combined with gradient method realized in ASSOL-2 software [17].

Different sets of data were examined. The best fit of the data was found in the case of simultaneous processing of the results [3,4,8,11] and the experimental

results of the present work. The total number of experimental points was 58 and gave a value of the object function of F=0.049. The following parameters were obtained:

$$\Phi_{12} = -79.987, \quad \Phi_{21} = -65.975,$$
$$C_1 = -10617.5, \quad C_2 = 2.9643$$

The results show (Fig. 2) that the Al–Ni melt has a strong association tendency. The mole fraction of the AlNi associates is 0.62 for the equiatomic composition at 1800 K. The shape of the associate concentration vs. concentration function is determined by the stoichiometry of the associate and thus corresponds to the phase diagram of the system.

The approximation of the experimental data and a comparison with the data which were not included in the fit is presented in Figs. 3–7.

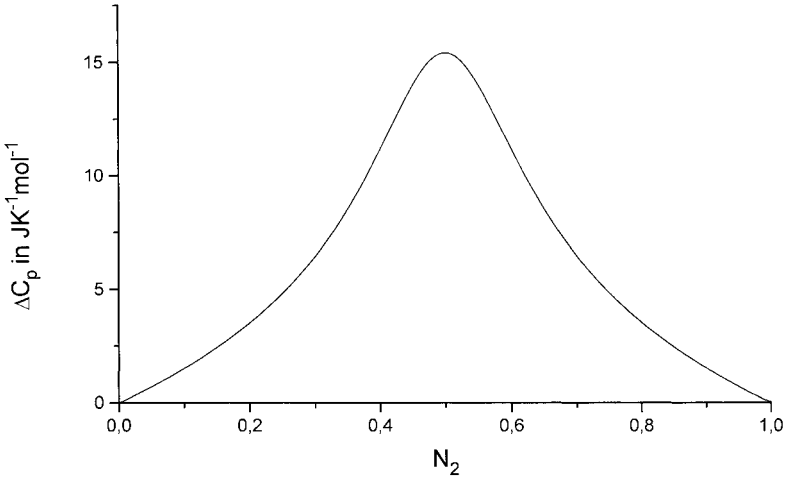

Fig. 8. Excess heat capacity ΔC_p of Al–Ni melt calculated by QIAS model at 1800 K.

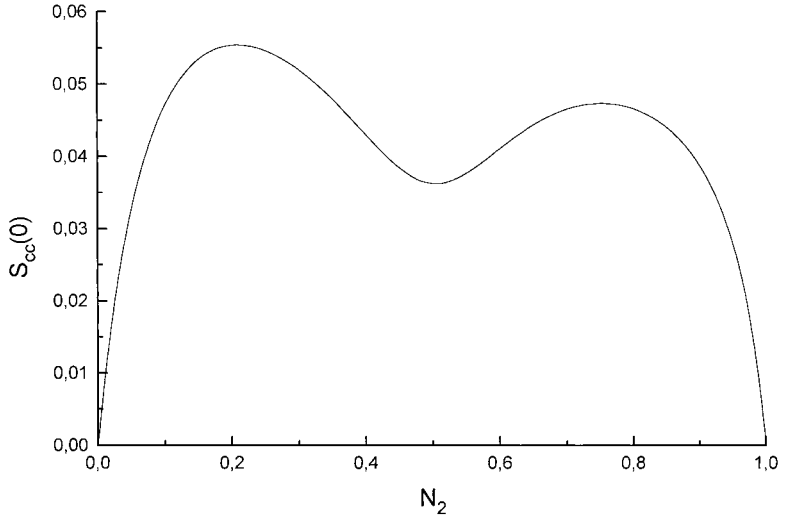

Fig. 9. The Bhatia–Thornton partial concentration structure factor in the long wavelength limit of Al–Ni melt calculated by QIAS model at 1800 K.

The excess heat capacity function ΔC_p and the Bhatia–Thornton partial concentration structure factor in the long wavelength limit $S_{cc}(0)$ at 1800 K are shown in Figs. 8 and 9, respectively.

4. Discussion

Al–Ni melts were investigated by different experimental methods. An approach with the QIAS model was used for comparative analysis of the available data sets.

The calorimetric studies of [4] at 1923 K, [10] at 1800 K, [13] at 1700 K and the experimental and calculated results of the present work at 1823 K are in a good agreement (Figs. 3 and 4). Only the partial enthalpy of mixing $\Delta\bar{H}_1$ [5] at 1873 K for N_{Al}=0.5 correlates with calculations and experimental results.

A difference of experimental and calculated partial enthalpies of Ni in dilute solution in Al at 1923 K (see Fig. 4) was found. This value needs additional experimental investigation, because the experimental $\Delta\bar{H}_2$ (N_{Ni}=0.02) =−149 kJ/mol at 1158 K [8] is in a good agreement with the calculated value of −152 kJ/mol. At the same time a slight temperature dependence of enthalpy functions was found in the all concentration intervals. The possible reason of the experimental error in this concentration region could be the overheating of the melt (more than 900 K over the liquidus line).

The data of [7] are less exothermic and the shape of the partial enthalpy function differs from the results of other authors.

The activity [6] at 1100 K, [11] at 1173 K (see Fig. 5) and [3] at 1873 K and the calculated curves are in a good agreement. The data of a Knudsen EMS investigation [12] at 1728 K differ from data [3] and the calculated curve (see Fig. 6). The data of a Knudsen EMS investigation [9] at 2000 K show too big deviations from ideal behavior (Fig. 7).

The excess heat capacity ΔC_p calculated at 1800 K is presented in Fig. 8. The values are close to the results of [13], where ΔC_p=14 J/mol K at 1700 K was found at the equiatomic concentration (14.87 J/mol K by our calculation).

The Bhatia–Thornton partial concentration structure factor in the long wavelength limit $S_{cc}(0)$ is very important for structure investigation of Al–Ni melts. Its values at 1800 K are shown in Fig. 9. The value of $S_{cc}(0)$=0.05 at 1330 K and N_{Ni}=0.2 differs from the thermodynamic estimation of $S_{cc}(0)$=0.15, used in the structure study [21].

5. Conclusions

Concentration dependencies of the partial and integral enthalpies of dissolution of aluminium were obtained experimentally in nickel-rich Al–Ni melts (N_{Al}<0.22) at 1823 K.

The model of quasi-ideal associated solutions and ASSOL-2 original software were used to treat and evaluate all available thermodynamic data for the liquid Al–Ni system.

The comparative analysis of the experimental data shows the reliability of the QIAS model description of the liquid Al–Ni alloys. The parameters of the model enable to find out thermodynamic properties of Al–Ni melt in a wide concentration and temperature region.

Acknowledgements

The authors express their thanks to L.S. Chistyakov and A.Ya. Stomachin for the participation in the calorimetric experiments.

References

[1] T.B. Massalski (Ed.), Binary Alloy Phase Diagrams, ASM Metal Park, Ohio, vol. 1, 1986, p. 140.
[2] N.P. Lyakishev (Ed.), Phase Diagrams of Binary Metallic Systems (Diagrammi sostoiania dvoinih metallicheskih system), Moscow, Mashinostroenie, vol. 1, 1996, p. 183 (in Russian).
[3] F. Vachet, P. Desre, E. Bonnier, C.R. Acad. Sci. 260 (1965) 453.
[4] V.M. Sandakov, Yu.O. Esin, P.V. Geld, Zh. Fiz. Chim., 45 (1971) 1798 (in Russian).
[5] O.I. Ostrovskii, V.V. Miasnikov, V.V. Pliushkin, A. Ya. Stomashin, V.A. Grigorian, Izv. Vuzov, Cher. Met., No. 11 (1976) 51 (in Russian).
[6] S.C. Shaefer, N.A. Gokcen, High Temp. Sci. 11 (1979) 31.
[7] N.V. Gizenko, S.N. Kilesso, D.V. Ilinkov, B.I. Emlin, A.L. Zavialov, Izv. Vuzov, Tsvet. Met., No. 4 (1983) 21 (in Russian).

[8] J.J. Lee, F. Sommer, Z. Metallkd. 76 (1985) 750.
[9] G.R. Johnson, L.D. Palmer, High Temp.–High Press. 12 (1980) 261.
[10] V.S. Sudovtseva, A.V. Shuvalov, N.O. Sharchina, Rasplavy, No. 4 (1990) 97 (in Russian).
[11] M. Bonnet, J. Roglz, R. Castanet, Thermochim. Acta 155 (1989) 39.
[12] K. Hilpert, M. Miller, H. Gerads, H. Nickel, Ber. Bunsenges. Phys. Ch. 94 (1990) 40.
[13] U.K. Stolz, I. Arpshofen, F. Sommer, B. Predel, J. Phase Equilibria 14 (1993) 473.
[14] P. Desai, J. Phys. Chem. Ref. Data 16 (1987) 109.
[15] L.S. Chistyakov, A.Ya. Stomachin, K.V. Grigorovitch, Izv. Ros. Akad. Nauk, Metally, No. 4 (1993) 27 (in Russian).
[16] A.S. Krylov, A.M. Katsnelson, V.I. Kashin, in: V.I. Kashin (Ed.), Interaction of Metallic Melts, Gas and Slags, Nauka, Moscow, 1986, p. 57 (in Russian).
[17] V.I. Kashin, A.M. Katsnelson, A.S. Krylov, Z. Metallkd. 81 (1990) 516.
[18] L.S. Darken, Trans. TMS–AIME 239 (1967) 80.
[19] A.B. Bhatia, D.E. Thornton, Phys. Rev. B8 (1970) 3004.
[20] A.S. Krylov, A.M. Katsnelson, Z. Metallkd. 84 (1993) 641.
[21] M. Maret, T. Pomme, A. Pasturel, P. Chieux, Phys. Rev. B42 (1990) 1598.